ELSEVIER

Catalysis Today 53 (1999) 207–223

CATALYSIS TODAY

www.elsevier.com/locate/cattod

NMR and modelling studies of structural heterogeneity over several lengthscales in amorphous catalyst supports

Sean P. Rigby *

Synetix, PO Box 1, Belasis Avenue, Billingham, Cleveland, TS23 1LB, UK

Abstract

In order to fully understand the operation of porous catalyst pellets in a reactor it is necessary to determine the influence of the complex structure of the pore space and void/solid matrix interface on the various chemical and physical processes taking place within the pellet. Recent developments in the formulation of structural representations of porous pellets that are more accurate over a wider range of lengthscales than in previous work have been discussed. A new model of interpretation for deuterium NMR data on the motion of benzene molecules on the surface of amorphous catalyst supports has been developed. The model, based on fractal concepts, has shown that the pre-exponential factor for an activated jump-type motion model correlates quantitatively with the degree of surface structural disorder, as characterised by the surface fractal dimension. This finding suggests a new way of measuring surface fractal dimension. This model has then been used to confirm the supposition that surface diffusing molecules effectively probe larger lengthscales as the temperature is increased.

Keywords: NMR; Amorphous catalyst; Structural heterogeneity

1. Introduction

Complex patterns of reaction behaviour are observed during catalyst operation. These phenomena include a particular activity, specific selectivities between competing reactions, kinetic phase transitions and oscillations. The specific features of the operation of a particular catalyst arise out of a combination of the different physical and chemical processes occurring over very different lengthscales in the catalyst pellet. Those processes are influenced by the catalyst pellet structure. The physical structure of individual catalyst pellets possesses high degrees of complexity over many lengthscales. This paper will, firstly, survey previous work attempting to formulate representations of catalyst pellet structure over all lengthscales and then describe some new work on the modelling of pellet structure and molecular dynamical processes occurring at the microscopic scale, which might be incorporated in such all-encompassing models.

Early work on the application of NMR methods [1–3] to the study of the structure of catalyst pellets indicated that they possess macroscopic (0.01–1 mm) heterogeneities in the spatial distribution of porosity and pore size. These heterogeneties were found to significantly influence the steady-state self-diffusion of water imbibed in the void space. The application of image analysis techniques to NMR images of the spatial distribution of pore size in catalyst pellets [4] offered various methods whereby the structural

* Tel.: +44-1642-522246; fax: +44-1642-522606
E-mail address: sean_p_rigby@ici.com (S.P. Rigby)

0920-5861/99/$ – see front matter
PII: S0920-5861(99)00117-0

disorder evident in the images could be characterised quantitatively. This finding offered the possibility of constructing models of catalyst pellets which were truly representative of the pellet structure over all lengthscales.

In a more recent study [5] the application of an image analysis technique developed in previous work [4] showed that the structure of many catalyst support pellets on the macroscopic scale is fractal in character. A fractal parameter obtained from NMR spin lattice relaxation time images (which probe pore size) was shown to be constant for pellets drawn from the same batch but to differ significantly between batches. It was suggested [5] that differing manufacturing methods imposed differing degrees of macroscopic heterogeneity on porous pellets. Previous experimental studies [2,3] had shown that measurements of an overall average value of tortuosity for the same liquid imbibed in the same porous solid from magnetic resonance imaging (MRI) and pulsed gradient spin echo (PGSE) NMR methods generally gave higher values of tortuosity using MRI than with PGSE NMR. Recent work [5] on the simulation of diffusion inside disordered porous media has suggested an explanation of this result. The two different experiments have quite different physical boundary conditions. In the case of an experiment which measures directly the self-diffusion coefficient (such as PGSE NMR) the results will be sensitive to molecules randomly exploring their local volume and in this case the molecules will tend to follow the path of least resistance. When the experiment involves a measurement under an applied concentration gradient (as in the MRI experiment) then the measured diffusive flux will be dependent on the net transfer of diffusing species within a generally macroscopic heterogeneous region. At a molecular level the diffusion may still be dominated by motion along the path of least resistance, but now additional tortuosity is introduced via heterogeneity on the larger scale as the molecular diffusive flux may alternatively be, relatively, reduced or enhanced during its passage through disparate regions of the sample, thereby leading to a lower experimental measurement of the diffusivity and hence higher value of tortuosity.

Early modelling work [6] had attempted to study the effect of disordered structures of fractal character on diffusion processes in catalysts. Structural characterisation studies using a variety of experimental techniques, such as gas sorption [7] and SAXS [8], have shown that some catalysts have a fractal structure on the microscopic scale ($<10\,\mu$m). In recent work [5], the previous modelling approaches [6] were extended to structural representations which attempted to incorporate pellet structural disorder on both the microscopic and macroscopic lengthscales in the form of composite cluster–cluster aggregate (CCA) models. These models consisted of a chessboard arrangement of individual CCA model structures (see Fig. 1). CCAs of two different voidage fractions were each allocated to the two sets of squares, denoted by ‘A’ and ‘B’ in Fig. 1. The degree of heterogeneity could be increased, while retaining a constant value of overall average porosity, by increasing the difference in the individual porosities allocated to the A and B sites. These models might represent porous catalyst pellets formed by a tabletting procedure where the pellet feed undergoes a precompaction step followed by fragmentation and the selection of a particular particle size range for the final compaction step. Under- and oversized particles are often recycled around the loop of precompaction and fragmentation, thereby presenting the possibility that a particular portion of feed might be precompacted many times and thus densified to a greater extent than other portions of the feed. Hence heterogeneity may be re-introduced at the macroscopic scale. Diffusion processes in the composite CCA structures were simulated by two different methods first proposed by Elias-Kohav et al. [6] called whole object averaging and diffusion flux. In the whole object averaging approach the local tortuosity is approximated by the number of sideways diversions that a molecule

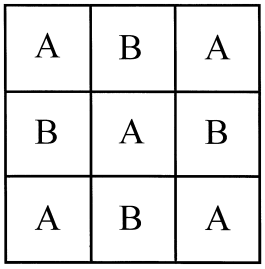

Fig. 1. A Composite CCA. In each of the regions labelled A and B, a single CCA structure is present; A and B have different voidage fractions [5].

needs to proceed in the void. In 3D, if M is the locally averaged number of blocked pixels adjacent to an empty site, then the probability of a one pixel diversion is $M/6$ (or $M/4$ in 2D). After such a move there is a similar probability of a further diversion and when M does not vary with every diversion the local tortuosity after n steps is

$$\tau = 1 + \left(\frac{M}{6}\right) + \left(\frac{M}{6}\right)^2 + \ldots + \left(\frac{M}{6}\right)^n \rightarrow \left(\frac{1}{1-(M/6)}\right) \quad (1)$$

in 3D, where the limit holds for large n. An analogous expression holds in 2D. The diffusion flux method simulates diffusion occurring under a concentration gradient, typical of a Wicke–Kallenbach experiment. The lattice occupied by the model structure is divided up into smaller boxes, squares (in 2D) or cubes (in 3D), and the voidage fraction and local tortuosity (found using Eq. (1) above) is found in each box. The steady-state diffusion equation for the appropriate geometry is then solved using a finite difference algorithm. A value for the effective diffusivity for the whole structure is obtained from the flux predicted by the simulation and thus a value of tortuosity is deduced. It was found that the diffusion flux approach consistently predicted higher values of tortuosity for composite CCAs compared to the whole object averaging method and this difference increased with increased model structural heterogeneity.

Recently [9] it has been shown in magnetic resonance imaging studies of the structure of a porous alumina tablet that macroscopic heterogeneities observed in the spatial distribution of voidage fraction and pore size directly influence the transient diffusional exchange of H_2O and D_2O. In a second study, it was found that differences in the image fractal dimensions characterising the heterogeneities observed in spin density images, which probe pellet porosity, of axial and radial planes of a cylindrical alumina tablet correlated with a difference in the tortuosities characterising transient diffusional liquid–liquid exchange in those planes of the pellet.

In the light of the previous work described above it has been suggested [10] that the total tortuosity of a porous pellet has independent contributions from tortuosity on various lengthscales. Previous studies of the simulation of diffusion in catalyst pellets has generally made use of abstract model representations of pellet structure. Magnetic resonance images of the spatial distribution of porosity within a thin slice through a porous catalyst support pellet were used [10] as the basis for more realistic representations of porous structures. Simulations of diffusion using the two different methods, diffusion flux and whole object averaging, on these image derived model structures were found to account quantitatively for the difference in the measured values of overall average tortuosity obtained from MRI and PGSE NMR methods.

Monte-Carlo simulations provide a powerful technique whereby the physical and chemical processes occurring during catalysis may be simulated. In the past, generally, simulations have treated catalysts as having regular, Euclidean-type geometry. More recently there have been attempts to incorporate the structural disorder present in real materials into the model catalyst. Monte-Carlo simulations have studied the influence of structural disorder on selectivity between competing reactions [11,12] and the catalytic oxidation of carbon monoxide [13]. Differential accessibility and connectivity (in the sense of numbers of nearest neighbours) of active sites significantly influences reaction behaviour. Very recently it has been recognised [14] that the convolutions of the catalyst surface over several different lengthscales each have an influence on the selectivity between reactions. It has been suggested [14] that the range of methods used to study structural disorder such as gas sorption or SAXS must be extended to include methods such as NMR imaging which are sensitive to structural features over larger lengthscales. Monte-Carlo simulations have suggested that heterogeneities in the spatial distribution of porosity and void surface area-to-volume ratio over lengthscales from $\sim$10 μm to $\sim$1 mm observed in NMR imaging studies of catalyst pellets significantly influence selectivity between competing three step reactions. Thus structural disorder and its effect on mass transport over a wide range of lengthscales will influence catalyst activity and selectivity. It has been found [14] that the selectivity between competing first and second order reactions correlates with both the voidage fraction and mass fractal dimension of the porous structure.

Recently Monte-Carlo simulations of surface reactions have incorporated surface diffusion phenomena

[15,16]. At the microscopic scale the rate of surface diffusion of species will also influence catalyst selectivity and activity. A model has been developed [17] to interpret the temperature dependence of the motional correlation time data derived from deuterium NMR relaxation time experiments for fully deuterated sorbed species on the surface of amorphous catalyst supports. A statistical description of the irregular surfaces based on fractal concepts is used in the development of a site-hopping model which relates the thermally activated jump processes occurring to the motional correlation times derived from the Lorentzian peak observed in deuterium NMR studies. Recent molecular dynamics simulations [18] have suggested that nearest-neighbour adsorbate hopping models of surface diffusion must be adapted to incorporate the multi-site hopping and longer flight processes that occur at higher temperatures. Evidence that molecules effectively probe larger lengthscales with increasing temperature has been found from a combination of deuterium NMR studies of molecular motion [17], and nitrogen sorption and mercury porosimetry studies of surface and pore structure. For molecules, such as benzene which interact with catalyst surfaces primarily via dispersion forces it has been found that the rate of site hopping correlates exactly with the degree of surface roughness over the lengthscales probed by the molecule at a particular temperature. For molecules which have a more specific interaction with the surface, such as water on silica, it has been found [17] that a further factor in the influence of surface irregularities on molecular motion is their effect in determining local surface chemistry of the catalyst surface.

This paper will concentrate on expanding earlier studies [17] of the influence of surface roughness and overall geometry on the motion of molecules adsorbed on the surface and interacting via dispersion forces. This paper, firstly, describes a theory of molecular motion on the surface of amorphous porous solids employing fractal concepts. Secondly, the predictions of the theory are compared with experimental results for real materials. These experimental results consist of the characterisation of surface and pore morphologies using nitrogen sorption and mercury porosimetry, and surface diffusion measurements for benzene on silicas using deuterium NMR.

2. Theory

2.1. Deuterium NMR

In this work the motion of fully deuterated benzene (C_6D_6) molecules on the surface of amorphous catalyst supports is considered. This section describes the relevant theory to enable information about the motion of the molecules to be extracted from deuterium NMR line spectra of the benzene. In order to obtain motional correlation time data for adsorbed molecules from deuterium NMR spectral line-shapes it is necessary to use a model for the motions exhibited by the molecule to relate the spin–spin relaxation time to the motional correlation time characterising the behaviour of the molecule. The spin–spin correlation time is inversely proportional to the full width at half maximum height of the Lorentzian peak in the spectrum. In this work the model used to relate spin–spin relaxation time to a correlation time, τ, assumes that two types of motion are occurring simultaneously. The first motion is an anisotropic motion about a preferred axis in the molecular frame, while the second is a motion which moves the C–D bond isotropically in space due to the movement of the whole molecule. In previous work [19] this second time constant was used to characterise translational motion between adsorption sites within a zeolite framework conditional on the fact that this motion occurred rapidly on the NMR timescale and resulted in isotropic averaging of the quadrupole tensor. Both the isotropic and anisotropic rotational motions may be regarded as activated processes which enable the corresponding correlation times to be expressed in Arrhenius form. Using this model, the following expression is obtained for the full width at half-height ($\delta\nu$) of the Lorentzian peak observed in deuterium line-shape studies:

$$\delta\nu = \left(\frac{9\pi}{80}\right)\left(\frac{e^2 q Q}{h}\right)^2 \tau \tag{2}$$

$$\tau = \tau^0 \exp\left(\frac{E}{RT}\right) \tag{3}$$

where τ is the correlation time contributing to the spin–spin relaxation, (e^2qQ/h) is the rigid deuterium quadrupole coupling constant for benzene, taken to be 187 kHz [20], R is the molar gas constant and T is the absolute temperature, and τ^0 and E are the

pre-exponential factor and activation energy characterising the thermally activated motion of interest.

In previous work on the motion of benzene in zeolites Alexander and Gladden [19] treated the activated process as a desorption from a given site, followed by one or more independent processes such as adsorption at another site in the same zeolite cavity or passage through a window in the zeolite cage by overcoming an additional activation energy barrier. If one type of motion which contributes to the relaxation of the deuterated species is considered then the effect of introducing the activated jump model is not to alter the interpretation of the type of jump, but rather the rate of jumping [19]. Alexander and Gladden [19] assumed that within the zeolite cage there are n sites between which jumps may be made leading to a line narrowing of the NMR signal, but that a molecule was not guaranteed of making such a jump between these sites. Thus the rate of the process, v, (and hence correlation time) depended only on the number of available sites such that

$$\tau = \left(\frac{1}{v}\right) = \left(\frac{\tau^0}{n-1}\right)\exp\left(\frac{E}{RT}\right). \tag{4}$$

In order to allow for the possibility of intercage jumps Alexander and Gladden [19] modelled a zeolite cage as having two types of sites: n sites per cage between which jumps lead to line narrowing and a second type of site (of population w) that were regarded as sites in the window between two cages. It was suggested [19] that this second type of site might be physically interpreted as the number of orientations that a molecule might take up while in transit through the window in the execution of an intercage jump process. It was also assumed that in order to perform a jump that lead to intercage motion an additional activation energy, Δ, was required. The probability of making an intercage jump, p_w, was taken to be proportional to $w\exp(-\Delta/RT)$. It was suggested that if a molecule was able to make intercage jumps then it would have an increased chance of making a successful line narrowing jump. The coordination number of the pore network was c. The number of sites that molecule could 'see' in adjacent cages was taken as cn and thus the motional correlation time of the molecule under consideration could be written as

$$\frac{1}{\tau} = (1-p_w)(n-1)\frac{\exp(-E/RT)}{\tau^0} + p_w cn\frac{\exp(-E/RT)}{\tau^0} \tag{5}$$

and if an explicit form for the probability is inserted the following is obtained:

$$\frac{1}{\tau} = \left[n\frac{\exp(-E/RT)}{\tau^0(1+w\exp(-\Delta/RT))}\right]\left[\frac{n-1}{n} + cw\exp\left(\frac{-\Delta}{RT}\right)\right]. \tag{6}$$

This form for the dependence of correlation time on temperature gave rise to three temperature regimes. In the limits of low, high and intermediate temperatures the following behaviour was anticipated:

$$\text{Low temperature}: \quad \tau \simeq \tau^0\frac{\exp(E/RT)}{n} \tag{7}$$

$$\text{High temperature}: \quad \tau \simeq \tau^0\frac{\exp(E/RT)}{(cn)} \tag{8}$$

$$\text{Intermediate temperature}: \ \tau \simeq \tau^0\frac{\exp((E+\Delta)/RT)}{cwn} \tag{9}$$

It can be noted from the form of these expressions that the rate of the process, $v(\propto 1/\tau)$, is proportional to the number of sites available for the molecule to jump to. In subsequent parts of this paper the contributions to the experimentally observed, lumped pre-exponential factor from the number of available jump sites, and other determining factors, such as motional geometrical/steric effects and molecular packing, will be treated together and referred to as τ^0. However, it is a further assumption of the theory presented here that the other determining factors that contribute to the pre-exponential factor (besides the number of available jump sites) are specific to a particular type of molecule-surface interaction only, and therefore do not vary where there are only differences in surface morphology alone. Zeolites are regular structures and have, relatively speaking, rigidly predictable surface structures. In a regular structure, such as a zeolite, the number of available sites is fixed by the exact geometry and chemistry of the lattice. In a more amorphous, irregular solid, such as silica, alumina or a carbon black, the sites available for a

particular molecule are not so regularly arranged as in a zeolite. The number of other sites adjacent to a particular site on the surface of a silica is not so ordered as with a zeolite. However, if it may be assumed that the surface perceived by the particular molecule is chemically homogeneous, then the number of available sites for a molecule to jump to is proportional to the area in its jump range. Thus

$$v \propto \frac{1}{\tau} \propto n \propto A \tag{10}$$

where n is now the number of accessible sites in the molecule jump range, L, and A is the area of solid surface in the molecule jump range. It is suggested that L is a representative jump lengthscale characteristic of a particular temperature for a given molecule.

Now, while the surface of an amorphous solid may appear rough and irregular it has been shown [7] that these apparently disordered surfaces often possess the property of self-similarity i.e. they are fractal in nature. As a consequence the degree of disorder can be characterised mathematically in the form of a fractal dimension. The roughness factor, r^{f}, is widely used in surface science and is defined as the ratio between the apparent surface area, A, as measured by an adsorption experiment, and the geometric area, A_{g} as seen under a microscope:

$$r^{\mathrm{f}} = \frac{A}{A_{\mathrm{g}}}. \tag{11}$$

Farin and Avnir [21] suggest that the roughness factor parameter will depend on the molecule used to determine A such that

$$\log\left(r^{\mathrm{f}}\right) = \left[\frac{2-d}{2}\right]\log(\sigma) \tag{12}$$

where σ is the cross-sectional area of the molecule used in the adsorption experiment and d is the surface fractal dimension. Thus the surface area within a given range L seen by an adsorbed molecule is given by

$$A = A_{\mathrm{g}}\sigma^{(2-d)/2}. \tag{13}$$

Now it has been stated above that the rate of the jumping process for a particular molecule is proportional to the number of available sites and hence the surface area within a particular jump range L. The situation where the same molecule is making jumps on two different surfaces at the same temperature will now be considered. If the temperature is the same it will be assumed that the particular jump range on both materials will be the same. However, if the two different materials, denoted by the subscripts 1 and 2, have differing degrees of surface roughness then the actual surface area within that jump range will be different. If both surfaces are fractal then the ratio of the surface areas from Eq. (13) will be given by

$$\log(A_1) - \log(A_2) = \left[\frac{2-d_1}{2}\right]\log(\sigma) - \left[\frac{2-d_2}{2}\right]$$
$$\log(\sigma) = \left[\frac{d_2-d_1}{2}\right]\log(\sigma). \tag{14}$$

It has also been stated above that the rate of hopping is proportional to the surface area of the solid on which the molecule is adsorbed. In the model of Alexander and Gladden [19] the dependency on the number of sites occurs in the pre-exponential factor. Thus combining Eqs. (10) and (14) gives an expression for the ratios of the pre-exponential factors actually observed:

$$\log(\tau_1^0) - \log(\tau_2^0) = \left[\frac{d_1-d_2}{2}\right]\log(\sigma). \tag{15}$$

Hence the ratio of the pre-exponential factors for the jump rate of a particular molecule of cross-sectional area σ on two structurally different but chemically similar surfaces is a function of the two surface fractal dimensions.

In previous work, such as that of Rolle-Kampczyk et al. [22], it has been observed for some surfaces that at a particular lengthscale R there is a crossover from a surface scaling characterised by a surface fractal dimension d to another scaling regime characterised by a different surface fractal dimension D. This means that at a level of inspection above a lengthscale R the surface would have a different surface area to that which might be anticipated had it retained the scaling behaviour prevalent below the lengthscale R. If the surface is envisaged to be tiled with notional molecules with a cross-sectional area equal to R^2 then, by analogy with Eq. (14), the ratio of the surface area which might be expected if the previous scaling regime had been retained (A_1) to the surface area occurring due to the change in scaling behaviour (A_2) is given by

$$\log(A_1) - \log(A_2) = (D-d)\log(R) \tag{16}$$

Now if the jump range of a surface diffusing molecule should be caused to extend beyond this critical lengthscale, R, by an increase in temperature then, since the jump rate is proportional to the surface area within that jump range, a change in the pre-exponential factor characterising the jump process might be anticipated such that

$$\log(\tau^0) - \log(\tau^{0'}) = (d - D)\log(R) \tag{17}$$

where the dash indicates the pre-exponential factor applying to jumps of length longer than R.

2.1.1. Measurement of surface fractal dimension

If the rate of surface diffusion is influenced by the degree of surface roughness, it is therefore necessary to find a means by which surface fractal dimensions may be measured. Pfeifer et al. [23] derived an expression for the surface fractal dimension from an analysis of multilayer adsorption to a fractal surface such that

$$\ln\left(\frac{V}{V_m}\right) = C + S\ln\left[\ln\left(\frac{P^0}{P}\right)\right] \tag{18}$$

where V is the volume of gas adsorbed at an equilibrium pressure P, V_m is the volume of gas in a monolayer, and P^0 is the saturation pressure. The constant C is a pre-exponential factor, and S is a power law exponent dependent on d, the surface fractal dimension, and the mechanism of adsorption. There are two limiting cases: at the lower end of the isotherm, representing the early stages of multilayer build-up, the film/gas interface is controlled by the attractive van der Waals forces between the gas and solid which tends to make the film/gas interface replicate the surface roughness. In this case the value of the constant S is given by

$$S = \frac{d-3}{3}. \tag{19}$$

At higher coverage, however, the interface is controlled by the liquid/gas surface tension (capillary condensation) which makes the interface move further away from the surface so as to reduce the interface area. In this second case S is given by

$$S = d - 3. \tag{20}$$

Under both circumstances the ratio V/V_m is related to the number of adsorbed layers, n, by

$$n = \left(\frac{V}{V_m}\right)^{1/(3-d)} \tag{21}$$

(Ismail and Pfeifer [24] suggest that the reason for $n > V/V_m$ when $d > 2$ is that fewer molecules are needed to form a multilayer of given thickness on a convoluted surface). In the intermediate regime both mechanisms will operate simultaneously and this may begin as early as the second layer, effectively making Eq. (19) unobservable, if the van der Waals attraction is weak. A slope S between $(d-3)/3$ and $(d-3)$ might then be expected. Therefore for any slope between -1 and 0 the inequality

$$3(1 + S) \leqq d \leqq 3 + S \tag{22}$$

will hold and, if the slope originates from the low coverage regime the following conclusions may be drawn from the difference $\delta = 3(1 + S) - 2$: (i) the actual d value, $d \geqq 2$, lies closer to 2 the smaller the absolute value of δ is. (ii) The effect of surface tension on S is negligible if $\delta \geqq 0$ and non-negligible if $\delta < 0$. Also, on a d-dimensional surface the theory [23] predicts the cross-over from the capillary condensation regime to the van der Waals regime at

$$\frac{V}{V_m} = \left[\frac{\alpha\rho}{(d-2)\gamma a^2}\right]^{(3-d)/2} \tag{23}$$

where α is the van der Waals constant for the gas/solid interaction, ρ is the number density of the liquid film, γ is the liquid/gas surface tension, and a is the thickness of one adsorbed layer. A low value of d shifts the onset of capillary condensation to higher V/V_m values.

It has also been proposed [7] that, for the pore-size distribution of a porous solid, the total volume of pores of diameters $\geqq 2r$, V_r, obeys

$$\frac{-\mathrm{d}V_r}{\mathrm{d}r} \propto r^{2-d} \tag{24}$$

where d is the fractal dimension of the pore surface. The surface fractal dimension may physically take values in the range $2 \leqq d \leqq 3$. Therefore, if the pore surface is fractal, a double logarithmic plot of $\log(V - V_r)$ against $\log(2r)$ will be linear with a slope of $(3-d)$. This equation is frequently applied to the analysis of pore-size distributions arising from nitrogen sorption capillary condensation region hysteresis loops and mercury porosimetry intrusion curves.

While both the theories implicit in Eqs. (18) and (24) describe the fractal surface they might be thought of as referring to different aspects of the surface structure. Ismail and Pfeifer [24] envisage that the hierarchy of pores implied by the fractal structure described by Eq. (18) may be visualised as a system of pit-like pores, with small pores being subpores of larger pores. Whereas the surface structure represented by Eq. (24) might be thought to describe the geometry of the mesopore network architecture.

3. Experimental

The samples studied in this work were two sol–gel silicas, G1 and G2, and a fumed (pyrogenic) silica, C1.

3.1. Deuterium NMR experiments

The silica samples were degassed at room temperature to at least 10^{-5} Torr before slowly being heated to 400°C over a period of approximately 1 h. The samples were then kept at that temperature under vacuum for 10 h. The sample was then cooled to room temperature before an amount of fully deuterated benzene (Aldrich HPLC grade with >99.5 at.% purity) equivalent to a monolayer coverage was adsorbed on the sample. The sealed sample was then placed in an oven at 60°C for 2 h to ensure homogeneous distribution of the benzene-D_6 in the sample. Deuterium NMR measurements were recorded on a Bruker MSL 200 NMR spectrometer operating at 30.72 MHz using a quadrupolar echo sequence with a 90° pulse of 6.9 ms and a time interval of 40 ms between pulses. Deuterium lineshapes of each sample were recorded at temperatures between 160 and 370 K. The temperature was stable to ±1 K. The number of echo signals accumulated depended on temperature, and varied between 100 scans at higher temperatures to about 50 000 scans at lower temperatures, with a repetition time of 0.5 s.

3.2. Nitrogen sorption

Nitrogen sorption experiments were carried out at 77 K by use of a Micromeritics ASAP 2000 apparatus. The sample tube and its contents were loaded into the degassing port of the apparatus and initially degassed at room temperature until a vacuum of 10^{-5} Torr was recorded. A heating mantle was then applied to the sample tube and the contents heated, under vacuum, to 100°C for 1 h. This procedure was repeated in 100°C steps until a final temperature of 400°C was reached. The sample was then left under vacuum overnight at a pressure of 6×10^{-6} Torr. At this point the heating mantle was removed and the sample allowed to cool down to room temperature. The sample tube and its contents were then reweighed to obtain the dry weight of the sample before being transferred to the analysis port for the automated analysis procedure. The sample tube was then immersed in liquid nitrogen at 77 K before sorption measurements were taken in the relative pressure region of $P/P^0 = 0.05$–1.00.

3.3. Mercury porosimetry

Mercury porosimetry measurements were made using a Micropore Autopore II 9220. The sample was first evacuated to a pressure of 50 mm Hg in order to remove the physisorbed water from the interior of the sample. The results were analysed according to the standard Washburn equation analysis.

4. Results and discussion

4.1. Deuterium NMR

For the temperatures when the deuterium spectrum was unequivocally a Lorentzian line the correlation times (obtained using Eq. (2)) are plotted against temperature for samples G1 and G2 in Figs. 2 and 3, respectively. Similar data for sample C1 have been reported by a previous worker [25]. The data for sample C1 were modelled by a single motional regime according to Eq. (3). The values reported for the motional pre-exponential factor and activation energy are given in Table 1. This data fit for C1 is shown as solid lines in Figs. 2 and 3. The correlation time data for samples G1 and G2 may also be modelled using a single motional regime. The parameters from Eq. (3) for this type of fit for G1 and G2 are also given in Table 1. However, in the case of sample G1, a better fit may be obtained to the data using a two motional regimes

Table 1
Fitted parameters for motional models of correlation time data for three silica samples

Sample	Temperature range (K)	Activation energy (kJ mol^{-1})	Pre-exponential factor (s)	Coefficient of determination (r^2)
C1[a]	200–330	20.7 ± 3.5	$1.04 \pm 0.19 \times 10^{-12}$	not reported [25]
G1	180–270	21.8 ± 1.0	$2.8 \pm 0.5 \times 10^{-13}$	0.9924
	180–210	16.8 ± 0.2	$6.6 \pm 0.1 \times 10^{-12}$	0.9999
	210–270	24.8 ± 1.1	$6.3 \pm 0.6 \times 10^{-14}$	0.9963
G2	190–290	21.7 ± 1.4	$4.4 \pm 1.2 \times 10^{-13}$	0.9825

[a] Notes: Obtained by a previous worker [25].

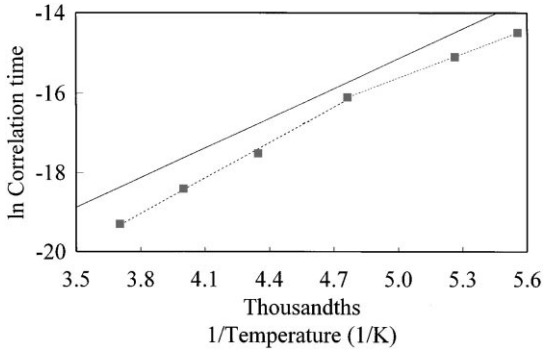

Fig. 2. Variation of benzene motional correlation time with temperature for sample G1. The solid line indicates a single motional regime model fit of Eq. (3) to data for sample C1 The dashed line indicates a two motional regime model fit of Eq. (3) to the data shown for G1.

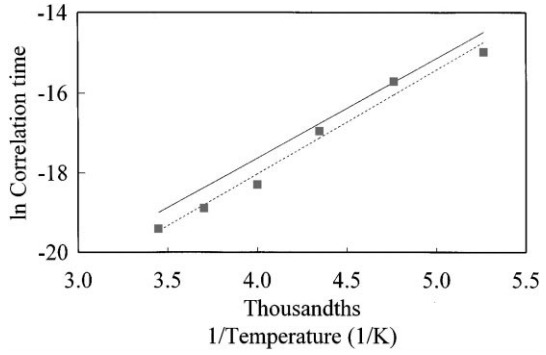

Fig. 3. Variation of benzene motional correlation time with temperature for sample G2. The solid line indicates a single motional regime model fit of Eq. (3) to the data for C1 The dashed line indicates a single motional regime model fit of Eq. (3) to the data shown for G2.

(above and below 210 K) model. The parameters from expressions of the form of Eq. (3) for this particular model fit are also given in Table 1. The coefficients of determination (r^2) for the different fits would indicate that, on purely statistical grounds, the two motional regime model gives a better representation of the correlation time data for sample G1 than the one motional regime model. However, it is the purpose of this paper to suggest that there are further reasons, beyond the merely statistical, for considering the two motional regime interpretation of the results for G1.

4.2. Nitrogen sorption

The data from the nitrogen adsorption isotherms for each of the samples C1, G1 and G2 are shown, in a form consistent with the terms in Eq. (18), in Fig. 4. Fig. 4 therefore shows a plot of ln(volume of nitrogen adsorbed) against ln(ln(1/relative pressure)). Fig. 4 also shows linear least squares regression straight line best fits to these data. The slopes (S) and coefficients of determination (r^2) for each of these fits are shown in Table 2. It can be seen from Fig. 4 and the values of r^2 quoted in Table 2 that the data give very good straight line fits over the ranges of relative pressure considered. Table 2 also shows the surface fractal dimensions calculated from the slopes of the fits according to both Eqs. (19) and (20). It can be noted that Eq. (19) yields too low a value of the surface fractal dimension to be physically meaningful (i.e. <2) over a wide range of coverages and without any departure from linearity. Ismail and Pfeifer [24] concluded that such behaviour indicated that the van der Waals regime is altogether suppressed, leaving Eq. (20) as the only possible explanation. The values of δ shown in Table 2 are all less than zero and thus, themselves, indicate a significant contribution from capillary condensation.

Table 2 shows the ranges of the number of adsorbed layers, corresponding to the ranges of relative pressures shown in Fig. 4 and calculated from Eq. (21) using the fractal dimensions from Eq. (20), considered

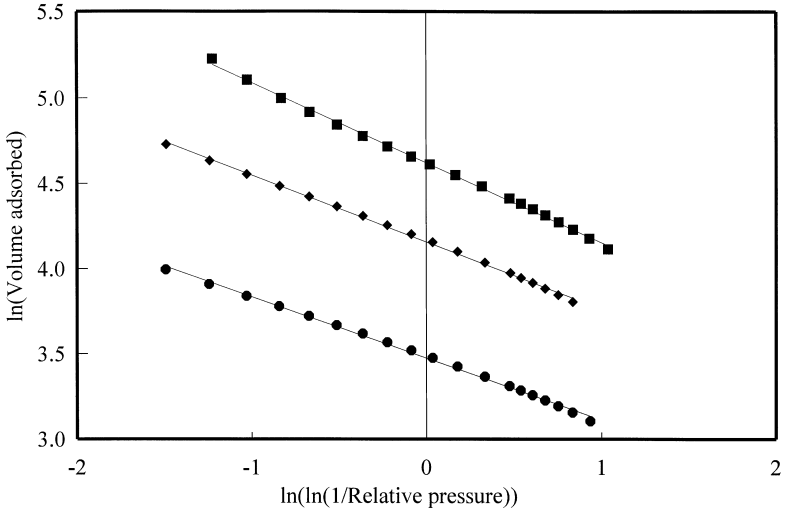

Fig. 4. Nitrogen adsorption data for silica samples Cl (◆),G1 (■) and G2 (●). The solid lines indicate fits of the data to Eq. (18).

for each sample. The actual thickness of coverage is obtained by multiplying by the diameter of the adsorbate molecule (0.35 nm for nitrogen). The lengthscale cutoffs encompassed by the surface fractal dimension is the thickness of the adsorbed multilayers over which the fractal dimension applies, and these values are also shown in Table 2. It can be seen that the range of the number of adsorbed layers considered is predominantly in the decade between 1 and 10 in all cases.

A further consistency test suggested by Ismail and Pfeifer [24] is to calculate, using Eq. (23), the value of V/V_m at which the crossover from the capillary condensation regime (Eq. (20)) to the van der Waals regime (Eq. (19)) occurs on each surface with fractal dimensions given by Eq. (20). Using the standard values of ρ and γ, as suggested by Ismail and Pfeifer [24], a value of $a = 0.35$ nm [24] and the value of α for nitrogen on glass calculated by Cheng and Cole [26] the value of V/V_m at the crossover is calculated to be $\sim$1 for all three samples. This would suggest that, considering the numbers of adsorbed layers studied (as calculated from Eq. (21)), the data employed here all lie, almost exclusively, in the capillary condensation regime and the use of the fractal dimension from Eq. (20) is justified.

The volumes of micropores for each sample were also obtained using a standard t-plot analysis and the t-layer thickness equation of Harkins and Jura [27]. These values are given in Table 2. It can be seen that the observed micropore volumes correlate well with the surface fractal dimensions from Eq. (20): a higher micropore volume is associated with a higher fractal dimension. This is what might be anticipated as a sample with a large micropore volume would be expected to be rougher over the lengthscales considered here.

Once measurements have been made of the surface fractal dimensions of two materials it is possible to make a prediction of the ratio of the pre-exponential factors for the motion of a particular molecule on the surface of those molecules using Eq. (15). In this work the molecule considered was benzene. The value taken for the cross-sectional area of the benzene molecule, σ, is 4×10^{-19} m^2 [28]. The ratios of the pre-exponential factors predicted for the various pairs of samples from the surface fractal dimension measurements are shown in Table 3. Also shown in Table 3 are the experimental results for this ratio found using the data given in Table 1. In the case of sample G1 it is the lower temperature range of the two motional regime model that is considered here. It can be seen from Table 3 that the model predictions follow the same trend as, and agree within the quoted error (i.e. the error bars overlap) with, the experimental measurements. These results would suggest that the premises on which the model is based are correct: the rate of the surface diffusion of a molecule is proportional to the number of

Table 2
Results of a fractal analysis of nitrogen sorption data for three silica samples

Sample	Range of relative pressures considered where fit to Eq. (18) is linear	Slope S, in Eq. (18)	Coefficient of determination (r^2)	Surface fractal dimension, d, from Eq. (19)	Surface fractal dimension, d, from Eq. (20)	δ	No. of adsorbed layers (obtained from Eq. (21))	Lengthscale cutoffs (nm)	Crossover V/V_m (obtained from Eq. (22))	Micropore volume ($cm^3\ g^{-1}$)
C1	0.100–0.799	-0.393 ± 0.004	0.9985	1.820 ± 0.001	2.607 ± 0.004	-0.179	1.017–10.710	0.356–3.748	1.1	0.003 ± 0.001
G1	0.060–0.746	-0.467 ± 0.005	0.9983	1.598 ± 0.002	2.533 ± 0.005	-0.401	0.764–8.232	0.267–2.881	1.1	~ 0[a]
G2	0.078–0.799	-0.360 ± 0.004	0.9978	1.911 ± 0.001	2.640 ± 0.004	-0.080	0.956–11.217	0.335–3.926	1.1	0.0045 ± 0.0007

[a] Note: No significant micropore volume observed.

Table 3
Comparison of predicted and experimentally measured values of the ratio of motional pre-exponential factors for combinations of three silica samples

Samples	Predicted ratio of pre-exponential factors (from Eq. (15))	Experimentally measured ratio of pre-exponential factors
G1 : G2	9.7 ± 1.8	15 ± 4
G1 : C1	4.81 ± 0.87	6.3 ± 1.2
C1 : G2	2.01 ± 0.34	2.36 ± 0.78

sites available for it to jump to (at a given temperature), which in turn is a function of the surface fractal dimension. It is also noted that the pre-exponential factor for the single motional regime model of the deuterium NMR data for sample G1 does not fit in so well with the theory predictions as that of the two motional regime model. The pre-exponential factor for the single motional regime model analysis of the data for G1 does not fit in so well with the generally observed correlation of increasing pre-exponential factor with decreasing surface fractal dimension. Thus the single motional regime model interpretation of the motional data for G1 is discounted.

It might be suggested that the differences in both the fractal dimension obtained from nitrogen adsorption and benzene hopping rate between the different silica surfaces may both be due to chemical heterogeneity instead of differences in geometrical structure. The consistency of the nitrogen adsorption and deuterium NMR experimental results described above suggests that, whatever its source, the heterogeneity is probed in a similar way using NMR and nitrogen adsorption. Even if all three silica samples had a planar surface the differences in benzene hopping rates, for the motional model described above, would also arise if benzene adsorbed onto specific sites on the surface and these sites existed in different concentrations on the different silica surfaces. Localized adsorption of nitrogen on specific sites of higher concentration on one silica compared to another could give rise to an apparently higher surface fractal dimension for that silica. Rouquerol et al. [29] state that the parameter C in the BET model for nitrogen adsorption can be defined as the ratio of the molecular partition functions for molecules in the first adsorbed layer and the liquid state existing above this layer. The parameter C is also exponentially related to the net molar energy of adsorption ($E^1 - E^L$) via the relation

$$C \simeq \exp\left[\frac{(E^1 - E^L)}{RT}\right]. \tag{25}$$

Rouquerol et al. [29] also suggest that if C (BET) has a value greater than 200 there is localized adsorption of nitrogen on specific sites. The values of C obtained from the BET model for samples G1, C1 and G2, after thermal pre-treatment to 400°C, are 75.3, 87.7 and 119.2, respectively. For all three samples the value of C (BET) is significantly less than 200 indicating that it is likely that no localized adsorption on specific sites occurs. In the case of mobile adsorption there is a random distribution of adsorbed molecules across the surface; whereas in the case of localized adsorption, the location of the adsorbed molecules is governed by the surface chemical structure of the adsorbent. It is also noted that an increasing value of C, and also the net molar energy of adsorption via Eq. (25), for nitrogen adsorption correlates well with increasing values of the activation energy for the hopping motion of benzene on G1 (two motional regime model), C1 and G2 in Table 1. The values of C are also sufficiently high that they are consistent with the suggestion of Rouquerol et al. [29] that for C (BET) > 50 there is no appreciable overlap between the completion of the nitrogen monolayer and multilayer development. Significant overlap occurs when there are relatively weak adsorbent–adsorbate interactions together with relatively strong adsorbate–adsorbate interactions. The values of C (BET) for the silica samples therefore suggest that the nitrogen adsorption data does indeed probe surface geometrical heterogeneity and differences in surface fractal dimension are not due to localized nitrogen adsorption at specific sites of differing concentration. In addition, Ismail and Pfeifer [24] suggest that for nitrogen coverages $V/V_m > 3$ specific adsorption sites would no longer influence the adsorption isotherm. The fractal scaling regimes obtained

from nitrogen adsorption on all three silica samples all extend well beyond values of $V/V_m = 3$ while retaining the same fractal scaling parameter as applies below that value.

Bilinski [30] proposes that benzene interacts with silica surfaces predominantly through dispersion forces. Bilinski [30] determined that the thermal pre-treatment of silicas provided almost no change in non-specific interactions with adsorbates, but did cause a considerable decrease in specific interactions such as acid–base ones. The elimination of active sites for specific adsorption was said to be due to the condensation of surface hydroxyls. If the adsorption of nitrogen on the silicas studied here was being influenced by specific interactions with the surface then it might be expected that the value of the surface fractal dimension obtained would decrease with increased temperature of the thermal pre-treatment of the silicas because the hydroxyl groups supposedly acting as specific adsorption sites would be progressively eliminated. DRIFT spectroscopy studies [17] of the three silica samples considered here have shown that the progressive elimination of surface hydroxyls does occur with an increasing temperature of thermal treatment. However, it can be seen from Table 4 that there is no significant variation of the measured surface fractal dimension with the temperature of thermal pre-treatment for all three silicas. These results suggest that the interactions of nitrogen with the moderately high temperature thermally treated surfaces studied here are non-specific.

The model considered above also assumes that the surface diffusing molecule interacts with the surface purely via dispersion forces with no chemical specificity for particular sites on the surface. Now, if the motional pre-exponential factor in Eq. (3) is assumed not to be (or only very weakly) a function of surface chemistry then the motional method might, therefore, be used to 'measure' the fractal dimension of other surfaces on which the mobility of benzene has been studied. Rouquerol et al. [29] surveyed the experimental results for the variation of low-coverage enthalpies of adsorption with both the carbon number and molecular polarizability for a wide range of polar and non-polar molecules (including benzene) on graphitized carbon black. These workers concluded that the linear relationships found are ample evidence to confirm the essentially non-specific nature of the interactions between the surface of graphitized carbon and all types of gas molecules. Grundke and Boddenberg [31] made deuterium NMR studies of the surface diffusion of benzene on a graphitized carbon black, and reported, for an expression analogous to Eq. (3), an activation energy of $3.8\,\mathrm{kJ\,mol^{-1}}$ and a pre-exponential factor of $3.33 \times 10^{-9}\,\mathrm{s}$. Using these data and the experimental measurements reported here for the surface fractal dimension and motional pre-exponential factor for sample C1 in Eq. (15) it is possible to estimate the surface fractal dimension of the graphitized carbon black sample used by Grundke and Boddenberg [31] as 2.226 ± 0.004. Nitrogen adsorption data for exactly the same sample as that used by Grundke and Boddenberg is not available to the author in order to confirm this prediction, however, Farm and Avnir [21] report surface fractal dimensions for similar materials: graphitized carbon black, 2.0–2.1; activated carbon fibres, 2.3 ± 0.2; carbon black, 2.25 ± 0.09 and graphon-vulcan 3G, 2.07 ± 0.01. The surface fractal dimension obtained here for the graphitized carbon black studied by Grundke and Boddenberg is similar to that for these other carbonaceous substances, and is less than that for the silicas studied here, as might be expected from the known mainly planar-type geometry of graphitic materials. TEM studies by Oberlin [32] have suggested that the structure of carbon blacks may contain various dislocations, defects and crumpled (rather than flat) lamella structures, depending on the degree of graphitization of the sample. The relatively high fractal dimension (compared to that for pure graphite) of the carbon black studied by Grundke and Boddenburg [31] may be due to incomplete graphitization of the sample. The possibility of using comparisons of the predictions of the non-chemically specific molecular motion theory described here for two chemically different materials with what is actually observed in order to extract information on the geometry of chemical heterogeneity of the surface and its interaction with various types of molecules is the subject of ongoing study. It is suggested that the geometric heterogeneity of a particular material might be characterised by one molecular species with non-specific interactions with the material surface. For another type of molecule with a specific interaction with the surface the influence of chemical heterogeneity might be deconvolved from structural effects by comparing

Table 4
A comparison of the results of the fractal analysis of nitrogen adsorption data for the three silica samples after thermal pre-treatment to different temperatures

Sample	Temperature of thermal pre-treatment (°C)	Surface fractal dimension	Lengthscale cutoffs (nm)
C1	350	2.614 ± 0.002	0.794–3.717
	400	2.607 ± 0.004	0.356–3.748
G1	200	2.537 ± 0.005	0.332–3.151
	300	2.525 ± 0.005	0.277–2.781
	350	2.505 ± 0.007	0.263–3.873
	400	2.533 ± 0.005	0.267–2.881
G2	300	2.658 ± 0.005	0.299–11.80
	350	2.62 ± 0.01	0.577–19.79
	400	2.640 ± 0.004	0.335–3.926

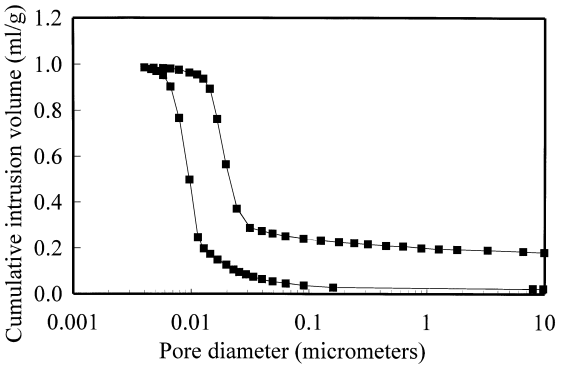

Fig. 5. Cumulative mercury intrusion and retraction curves for sample G1.

the motion of the two different molecules on that surface.

4.3. Mercury porosimetry

Fig. 5 shows the cumulative intrusion and retraction curves for a mercury porosimetry experiment on sample G1. Fig. 6 shows a plot of the logarithm of the total pore volume minus the pore volume of pores of diameter greater than a diameter d, against the logarithm of the diameter d obtained from the results of mercury intrusion porosimetry for sample G1. Fig. 6 also shows a linear least squares linear regression for the data between pore diameters of 11.4 and 33.5 nm. The coefficient of determination (r^2) for the fit is 0.93, indicating a reasonable fit to a straight line. Analysis of this fit according to the model described by Eq. (24) suggests a surface fractal dimension of 2.82 ± 0.02 for the surface of G1 between the aforementioned lengthscale cutoffs. An identical value (2.816 ± 0.002) has been obtained previously [17] using the same analysis method on the nitrogen desorption BJH pore-size distribution between lengthscale cutoffs of 11–55 nm. In both cases the results satisfy the minimal condition suggested by Pfeifer [33] for a 'well-defined' fractal dimension. These results indicate that (at least) above $\sim$11 nm the fractal scaling of the surface of sample G1 has changed scaling parameter. As has been mentioned previously in the theory section above, if such a situation should arise a change in motional pre-exponential factor would be anticipated in accordance with Eq. (17). The deuterium NMR results indicate that such a change in motional pre-exponential factor does occur for G1 around 210 K. Using the fractal dimensions obtained from nitrogen adsorption and mercury porosimetry for G1 and a transition lengthscale, R, of 11.4 nm in Eq. (17) it is possible to predict the change in motional pre-exponential factor expected to arise in connection with the change in scaling behaviour. The prediction made for $\tau^0/\tau^{0'}$ using Eq. (17) is 195 ± 85. The actual value measured experimentally for this ratio is 104 ± 10. The prediction and measured value agree within the quoted experimental errors (i.e. the one standard error bars overlap). The agreement between theory and experiment is actually quite pleasing because Eq. (17) involves a power law and there is an unknown error in the value of the fractal dimensions obtained from the nitrogen desorption and mercury porosimetry experiments appearing in the power due to percolation effects. Since Eq. (24) is a power law the value obtained for the surface fractal dimension is very sensitive to small shifts in

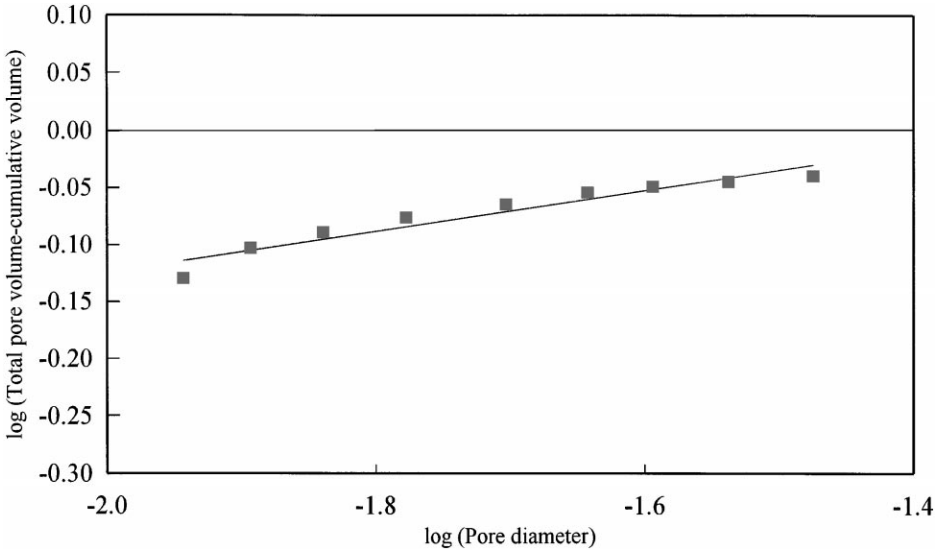

Fig. 6. Mercury porosimetry data for sample G1. The solid line indicates a fit of the model described by Eq. (24).

the experimental data. So-called 'shadowing' of large pores by small pores in these types of experiments causes a shift in the perceived pore-size distribution to smaller pore sizes. However the entrapment in the porosimetry experiment for G1 is small (∼16%) and hence the unknown systematic error is anticipated to be small because a small mercury entrapment is generally associated with only a small shift in the pore-size distribution [34]. The slight curvature evident in the data in Fig. 6 probably results from a non-negligibly small influence of a non-zero lower lengthscale cut-off in fractal scaling (contrary to what was assumed in the subsequent analysis of the data). However, the curvature is very slight (as shown by the high value of r^2) and was thus neglected here.

It will now be considered why a change in motional pre-exponential factor occurs at a lower temperature for G1 than for C1 and G2 (otherwise such a similar change would be evident in the data for C1 and G2 given in Figs. 2 and 3). It is suggested that this is because a change in fractal scaling is associated with a particular change in the overall void space-solid matrix interface geometry. Fig. 7 shows the cumulative nitrogen adsorption and desorption BJH pore-size distributions for samples Cl, G1 and G2. It can be seen that a dramatic step transition occurs in pore volume for the nitrogen desorption data for sample G1 at around 11 nm. A similar transition occurs in the analogous nitrogen adsorption data for sample G1 at a slightly larger lengthscale. This discrepancy may arise out of thermodynamic and/or percolation effects [29] but it must be noted from Fig. 7 that no such dramatic transition occurs at all for sample C1, and only occurs at a much larger lengthscale (>50 nm) for sample G2. It is suggested that the change in molecular motion occurs when the molecule changes from only exploring the pits on the surface of individual 'pores' and begins to explore the geometry of the pore network architecture itself, to some extent, as well. By analogy with the jumping motion of molecules through a window in a zeolite cage, this process also requires an extra activation energy as illustrated by the values given in Table 1 for the two motional regimes for sample G1.

Rolle-Kampczyk et al. [22] have proposed a hierarchical structure for sol–gel silicas where primary spherical silica particles aggregate to form nearly spherulitic secondary particles. In the light of this model, it is suggested that the fractal dimension measured by nitrogen adsorption on the silica samples characterises the surface roughness of the primary particles. In contrast, the fractal dimension obtained from mercury porosimetry characterises the geometry of the packing of the primary particles, which results from the nature of the process by which the

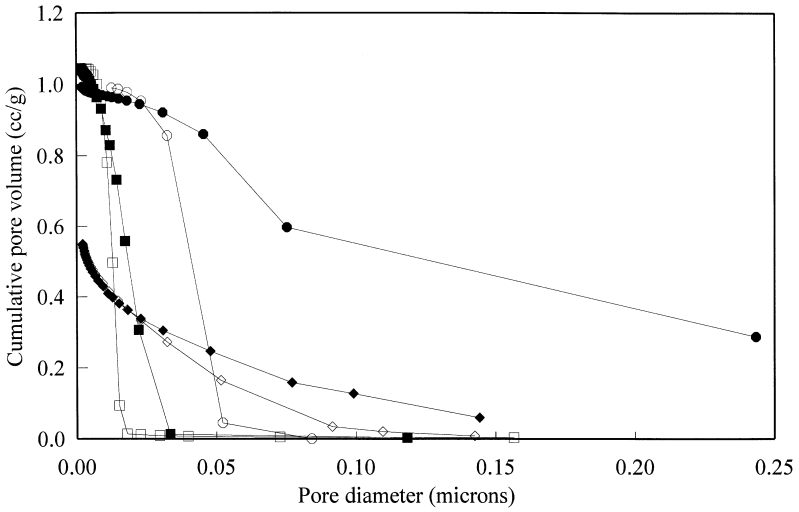

Fig. 7. Nitrogen sorption cumulative BJH pore-size distributions for samples C1 (diamonds), G1 (squares) and G2 (circles). The solid symbols indicate adsorption data and the open symbols indicate desorption data. The lines shown are to guide the eye.

secondary aggregates were created. The primary particle surface morphology and the pore system architecture in the secondary aggregates were probably created by very different physical processes and thus may be characterised by different fractal dimensions.

The mean diameter of the pore system created by the primary particles is nearly equivalent to the size of these particles [22]. This pore system is the particular structure probed by mercury porosimetry and BJH analysis of the nitrogen desorption branch of the sorption isotherm. It is suggested that a cross-over in fractal scaling might occur at a lengthscale characteristic of the pore system in the secondary aggregates. This characteristic lengthscale will approximately correspond to the sudden transition in the nitrogen desorption cumulative pore-size distribution or the turning point in the mercury intrusion curve. The data shown in Figs. 5 and 7 suggest that this lengthscale is in the range ∼6–11 nm. The uncertainty in this cutoff is, however, subsumed in the error quoted above for the ratio of pre-exponential factors calculated from the mercury porosimetry data using Eq. (17).

The hierarchical model for the silica structure also suggests that the surface tension effects in the nitrogen adsorption results may originate from capillary condensation at the necks (points of contact, wedge wetting etc.) between adjacent primary particles rather than capillary condensation, or surface tension effects, across the whole surface.

5. Conclusions

Porous catalyst support pellets possess complex and convoluted void structures over many lengthscales. In order to gain a full understanding of all the physical and chemical processes, and their interactions, which take place inside catalyst pellets during reactor operation it is necessary to include structural properties over all lengthscales in models of pellet performance. At the microscopic scale, the rate of surface diffusion of molecules is influenced by the degree of surface roughness of the solid/void space interface. For fractal surfaces it has been found that the surface diffusion rate correlates quantitatively with the degree of structural disorder characterised by the fractal dimension. This finding has also lead to a confirmation of the fact that the surface diffusing molecules effectively probe longer lengthscales as temperature is increased.

References

[1] M.P. Hollewand, L.F. Gladden, J. Catal. 144 (1993) 254.
[2] M.P. Hollewand, L.F. Gladden, Chem. Eng. Sci. 50 (1995) 309.

[3] M.P. Hollewand, L.F. Gladden, Chem. Eng. Sci. 50 (1995) 327.
[4] L.F. Gladden, M.P. Hollewand, P. Alexander, A.I.Ch.E. J. 41 (1995) 894.
[5] S.P. Rigby, L.F. Gladden, Chem. Eng. Sci. 51 (1996) 2263.
[6] T. Elias-Kohav, M. Sheintuch, D. Avnir, Chem. Eng. Sci. 46 (1991) 2787.
[7] P. Pfeifer, D. Avnir, J. Chem. Phys. 79 (1983) 3558.
[8] D.W. Schaefer, E.J. Martin, P. Wiltzius, D.S. Cannel, Phys. Rev. Lett. 52 (1984) 2371.
[9] S.P. Rigby, K. Cheah, L.F. Gladden, Appl. Catal. A144 (1996) 377.
[10] S.P. Rigby, L.F. Gladden, J. Catal. 173 (1998) 484.
[11] P. Meakin, Chem. Phys. Lett. 123 (1986) 428.
[12] C.K. Lee, S.L. Lee, Surf. Sci. 339 (1995) 171.
[13] H. Park, H. Kim, S. Lee, Surf. Sci. 380 (1997) 514.
[14] S.P. Rigby, L.F. Gladden, J. Catal. 180 (1998) 44.
[15] J. Mai, W. von Niessen, A. Blumen, J. Chem. Phys. 93 (1990) 3685.
[16] R. Chakarova, Surf. Sci. 389 (1997) 234.
[17] S.P. Rigby, L.F. Gladden, Stud. Surf. Sci. Catal. 122 (1999) 183.
[18] J.S. Raut, K.A. Fichthorn, J. Chem. Phys. 103 (1995) 8694.
[19] P. Alexander, L.F. Gladden, Zeolites 18 (1997) 38.
[20] B. Boddenberg, R. Burmeister, Zeolites 8 (1988) 488.
[21] D. Farin, D. Avnir, The fractal nature of molecule-surface interactions and reactions, in: D. Avnir (Ed.), The Fractal Approach to Heterogeneous Chemistry, Wiley, New York, 1989, p. 271.
[22] U. Rolle-Kampczyk, J. Karger, J. Caro, M. Noack, P. Klobes, B. Rohl-Kuhn, J. Colloid Interface Sci. 159 (1993) 366.
[23] P. Pfeifer, Y.J. Wu, M.W. Cole, J. Krim, Phys. Rev. Lett. 62 (1989) 1997.
[24] I.M.K. Ismail, P. Pfeifer, Langmuir 10 (1994) 1532.
[25] P. Chiaranussati, Ph.D. Thesis, Cambridge University, 1993.
[26] E. Cheng, M.W. Cole, Phys. Rev. B 38 (1988) 987.
[27] W.D. Harkins, G. Jura, J. Am. Chem. Soc. 66 (1944) 1366.
[28] S.J. Gregg, K.S.W. Sing, Adsorption, Surface Area and Porosity, Academic Press, London, 1982.
[29] F. Rouquerol, J. Rouquerol, K. Sing, Adsorption by Powders and Porous Solids: Principles, Methodology and Applications, Academic Press, London, 1999.
[30] B. Bilinski, J. Colloid Interface Science 201 (1998) 180.
[31] V. Grundke, B. Boddenberg, Molec. Phys. 79 (1993) 1215.
[32] A. Oberlin, High-resolution TEM studies of carbonization and graphitization, in: P.A. Thrower (Ed.), Chemistry and Physics of Carbon, vol. 22, Marcel Dekker, New York, 1989.
[33] P. Pfeifer, Appl. Surf. Sci. 18 (1984) 146.
[34] R.L. Portsmouth, L.F. Gladden, Chem. Eng. Sci. 46 (1991) 3023.